https://doi.org/10.5194/wes-2026-71
Preprint. Discussion started: 29 May 2026

eawe european academy of wind energy
Open Access WIND ENERGY SCIENCE DISCUSSIONS

Investigation of higher order statistics in wind turbine wakes using Large Eddy Simulations

Marcel Bock[1] and Joachim Peinke[1]

[1]ForWind – Institute of Physics, University of Oldenburg, Oldenburg, Germany

Correspondence: Marcel Bock (marcel.bock@uol.de)

Abstract. Large eddy simulation (LES) of the turbulent wake behind a wind turbine is employed to obtain a more complete statistical characterisation. Both one- and two-point statistics are therefore considered, including velocity increments. The downstream evolution of the wake size is determined by different statistical quantities, including the intermittency ring. Higher-order statistics show that the wake expands beyond the region commonly defined using the mean wind speed. Regarding the numerical simulations, a new method is introduced to reduce the computational cost of high-resolution wake simulations. This method can reduce the computational cost of the main simulation by approximately 20%.

1 Introduction

The rapid expansion of offshore and onshore wind farms causes the influence of wind turbine wakes on other turbines to become increasingly important. Therefore, detailed knowledge of turbine wakes is essential for the optimal placement of wind turbines, as this is a crucial factor affecting both the energy production and structural integrity. It is the wake that leads to a reduction of the wind speed, increased unsteady aerodynamic loading and accelerated fatigue damage (Bartl et al., 2012).

Wake modelling for wind energy applications has traditionally focused on the mean velocity (deficit) and the turbulence intensity (TI), which governs power losses and recovery rates. Analytical and engineering wake models, such as the Gaussian (Bastankhah and Porté-Agel, 2014) and double-Gaussian (Schreiber et al., 2020) wake formulations, have become widely used due to their simplicity and computational efficiency. These models describe the spatial distribution of the mean streamwise velocity and have been successfully calibrated against experimental and numerical data, but they generally neglect higher-order flow statistics and particular temporal variability. However, it is well known that turbulence requires a detailed description based on higher-order statistics. Neglecting this may lead to inaccuracies in predicting fatigue loads, as unsteady flow features are increasingly recognized as critical drivers of turbine fatigue (Chamorro and Porté-Agel, 2009; Lee et al., 2012; Guma et al., 2021). Ali et al. (2016) were the first to study higher-order velocity moments in wind turbine wakes. However, this analysis was limited to a single line downstream of a turbine array and primarily focused on the structure functions. In the present study, higher-order moments are analysed in greater detail for a single turbine and related to the Gaussian wake model.

The incoming flow field, being the turbulent atmospheric boundary layer or a wake, experienced by a wind turbine is inherently unsteady and complex, influenced by fluctuating wind directions and various other characteristics of the turbulent atmospheric boundary layer (Porté-Agel et al., 2011; Sanchez Gomez and Lundquist, 2020; Lledó et al., 2019). Understanding these effects

https://doi.org/10.5194/wes-2026-71
Preprint. Discussion started: 29 May 2026

eawe european academy of wind energy
Open Access WIND ENERGY SCIENCE DISCUSSIONS

therefore requires consideration of higher-order statistical moments.

An essential component of turbulence is the so-called small-scale intermittency, defined as the non-Gaussian distribution of velocity increments on small scales, meaning that extreme velocity events occur more frequently, see Frisch (1995). Note that in atmospheric turbulence, this small-scale turbulence is present on scales of the size of a wind turbine (Boettcher et al., 2003). These extreme events have been identified as important drivers of wind turbine loads (Mücke et al., 2011; Schwarz et al., 2019). Recent experimental observations have revealed the presence of a pronounced intermittency ring in turbine wakes, with even more extreme events compared to atmospheric turbulence alone, as determined by λ^2 (Neunaber, 2019; Vinnes et al., 2023; Zheng et al., 2023). In the present study, this characterization is extended through the determination of the intermittency parameter μ. This ring-like structure lies outside the ring of enhanced turbulent intensity near the wake shear layer and indicates regions of intense rotational and straining motions. The intermittency ring has been shown to coincide with zones of enhanced unsteady loading (Schottler et al., 2018), suggesting a direct link between small-scale turbulence dynamics and the turbine's structural response. Despite its apparent relevance, the downstream evolution of this intermittency ring and its connection to the wake recovery have not been investigated in detail.

The present study addresses these gaps by investigating velocity-related quantities beyond the mean velocity and TI in wind turbine wakes. It examines the higher moments of the velocity in Sect. 4.1. The self-similar velocity and TI profiles are extended by the skewness and kurtosis (Sect. 4.2). Then the velocity increments and the intermittency ring are investigated in Sect. 4.3. Finally, the downstream evolution of the wake expansion and the intermittency ring are compared in Sect. 4.4. This first combination of classical wake models with the intermittent ring paves the way for a unified wake expansion model. Such a model is important for wind farm design, as it could provide a more accurate prediction of turbine loads.

Furthermore, a novel method for simulating turbulent wakes is introduced. By sampling a laminar wake and superposing it onto a turbulent wind field, a computationally efficient and realistic wake flow is obtained for numerical simulations.

2 Fundamentals

This section outlines the fundamental concepts relevant to the present study. Specifically, computational fluid dynamics is introduced in Sect. 2.1, intermittent turbulence is discussed in Sect. 2.2, and synthetic turbulence is presented in Sect. 2.3. This overview is followed by the selection of the relevant settings in Sect. 3.

2.1 Computational Fluid Dynamics

The velocity $\mathbf{U}$ and kinematic pressure p (pressure normalized by density) of an incompressible flow field can be described by the Navier-Stokes equations

$$\nabla \cdot \mathbf{U} = 0, \tag{1}$$

$$\partial \mathbf{U}/\partial t + \big(\mathbf{U} \cdot \nabla\big)\mathbf{U} = -\nabla p + \nabla \cdot (\nu_{eff}\, \nabla \mathbf{U}) + \mathbf{F}. \tag{2}$$

https://doi.org/10.5194/wes-2026-71
Preprint. Discussion started: 29 May 2026

eawe european academy of wind energy
Open Access WIND ENERGY SCIENCE DISCUSSIONS

ν_{eff} represents the effective viscosity, which is the sum of the kinematic viscosity and the turbulent viscosity from the turbulence model ($\nu_{eff} = \nu + \nu_t$). In this work, a large eddy simulation (LES) is utilized, where the turbulent viscosity is calculated from the velocity field using an algebraic equation (further details are presented in 3.1). **F** denotes the source term for the integration of external forces such as gravity. Apart from physically present forces, this source term could be used in other ways. One is to model a wind turbine with actuator lines, which avoids computationally expensive representation of the blades, making it more suitable for large-scale simulations (Sørensen and Kock, 1995). Accordingly, the lift and drag forces generated by the blade elements are imposed on the flow field based on blade element theory (Froude, 1878).

2.2 Turbulent analyses

Due to the complexity of turbulent flows, they are described statistically. A key criterion is the level of detail in the statistical characterization. For simple wake studies, evaluating the mean value is sufficient. However, in the case of turbulence, a more advanced step-by-step analysis must be carried out, as demonstrated by Morales et al. (2012) and Fuchs et al. (2022). This begins with the lower moments of the one-point statistics, moves on to the higher moments, and continues with the two-point statistics, which must also be analysed in ascending order of the moments. Here, we restrict our discussion to the velocity component in flow direction, as commonly done.

The one-point statistics of (componentwise) velocity values U are completely described by the probability density function (PDF) $p(U)$. This probability is fully characterized, in the Gaussian case, by its mean value $< U >$ and variance $< u'^2 >$. Here $u' = U - < U >$, and $< u'^2 >$ is equivalent to the turbulence intensity, $TI := \sqrt{< u'^2 >} / < U >$. Gaussian probabilities are typically obtained for periods of constant wind speed in the unperturbed wind fields. This may change if extra shear is present, as in the case of wake flows. In this case, higher-order moments $< u'^n >$ become of interest.

Two-point statistics deal with velocity increments on the scale τ, defined as the change in velocity within this period of time

$$v(\overrightarrow{x}, t, \tau) = u'(\overrightarrow{x}, t+\tau) - u'(\overrightarrow{x}, t). \tag{3}$$

This definition of a velocity increment is based on Taylor's frozen turbulence hypothesis (Taylor, 1938), which replaces the original spatial separation with a temporal lag. The statistics are again given by the corresponding PDF $p(v(\tau))$. As by definition the mean value $< v(\tau) >= 0$, for a stationary flow, it remains to know the variance $< v(\tau)^2 >$ and the form of the distributions. It is a remarkable feature of turbulence that variance and form are scale-dependent, i.e. depend on τ.

The scale dependency of the variance is given by Kolmogorov's theory (K41) (Kolmogorov, 1941) with $< v(\tau)^2 > \propto \tau^{2/3}$. According to the Wiener–Khinchin theorem, this corresponds to the $f^{-5/3}$ decay of the power spectrum of $u(t)$. It has been shown within Kolmogorov's refined similarity hypothesis (K62) (Kolmogorov, 1962; Obukhov, 1962) that the velocity increments are Gaussian-distributed on large scales, but small scales within the inertial subrange exhibit an increased probability of extreme events. These heavy-tailed or intermittent distributions can be explicitly described using Castaing's model (Castaing et al., 1990)

$$p(v(\tau)) = \frac{1}{2\pi\lambda(\tau)} \cdot \int_0^\infty \frac{d\sigma}{\sigma^2} \exp\left[-\frac{v^2(\tau)}{2\sigma^2}\right] \exp\left[-\frac{\ln^2(\sigma/\sigma_0)}{2\lambda^2(\tau)}\right], \tag{4}$$

https://doi.org/10.5194/wes-2026-71
Preprint. Discussion started: 29 May 2026

eawe european academy of wind energy
Open Access WIND ENERGY SCIENCE DISCUSSIONS

which is equivalent to Beck's superstatistics (Beck, 2004). Whereby σ_0 determines the variance and λ^2 is an important parameter for the shape of the PDF. The Castaing model displays a Gaussian distribution for $\lambda^2 = 0$ and an intermittent distribution for $\lambda^2 > 0$. Instead of a fit of Eq. (4) to the PDF, the shape parameter can be calculated from the kurtosis of the increments directly, as shown by (Chilla et al., 1996) and (Beck, 2004)

$$\lambda^2(\tau) = \frac{\ln(\,\mathrm{Kurt}(\,v(\tau)\,)/3)}{4}. \tag{5}$$

This allows not only the description of the scale-dependent (τ-dependent) increment distributions, but also establishes a connection to the K62 model, which is commonly known as the log-normal model of turbulence. The K62 model describes the deviation of local energy dissipation from the average dissipation using the intermittency parameter μ. This can also be determined from the velocity increments using the shape parameter λ^2

$$9\lambda^2(\tau) = \Lambda_0^2 - \mu \cdot \ln(\tau). \tag{6}$$

This law for λ^2 is consistent with the scaling of higher order moments $< v(\tau)^n > \propto \tau^{\xi_n}$ (Castaing et al., 1990). Thus, we can also claim that λ^2 characterises all higher order statistics of the velocity increments. It is important to note that, based on our discussion here, this law (Eq. (6)) with the main parameter μ allows the complete two-point statistics $p(v(\tau))$ to be determined for any value of τ via Eq. (4).

As a last point of the topic of turbulence characterisation, we want to comment on the use of the term intermittency. One has to pay attention that intermittency is used in many different ways, here we focus on two intermittency aspects. First, a probability deviating from Gaussian shape is called intermittent if heavy tails are present so that the probability of large events is higher than for a Gaussian statistics. This effect is measured by the λ^2-parameter for increment statistics or by kurtosis for other statistics. In particular for turbulent signal there is a second phenomenon called intermittency, that is a change of the statistics with a scale from Gaussian to intermittent distributions. For turbulence (similar for general superstatistics) this change of the statistics can be parametrised by the intermittency parameter μ. In this sense, $\lambda^2 \neq 0$ as well as $\mu \neq 0$ characterises these two intermittency effects.

2.3 Synthetic turbulence

Synthetic turbulence is an established tool for generating turbulent fluctuations for numerical simulations. The basic idea originates from Veers (1984) and is based on spectral descriptions of the energy cascade (e.g. from Von Karman (1948). The fluctuations are modelled in Fourier space and then transferred to three-dimensional space. Due to this effectiveness and the reproducibility of the generation of inlet conditions, this methodology is prescribed in the IEC standard (IEC, 2019) for the design of wind turbines. This standard specifies models and values for its parameterisation. One of these is the Mann model (Mann, 1994, 1998), which is also used in this work. This model generates a vector field of velocity fluctuations and only needs to be parameterised with three values. These are the integral length, the turbulence intensity and a parameter for the shear.

https://doi.org/10.5194/wes-2026-71
Preprint. Discussion started: 29 May 2026

eawe european academy of wind energy
Open Access WIND ENERGY SCIENCE DISCUSSIONS

3 Methodology

In this section, the selected methodology for the study is explained and builds upon the previously introduced fundamentals. The investigation in this work is carried out with the NREL 5 MW reference turbine (Jonkman, 2009) in a turbulent environment at rated operating conditions ($U_\infty = 11.4\,\mathrm{m\,s^{-1}}$, ω_{rotor} = 12.1 rpm). It is commonly used in scientific studies and has a diameter D of 126 m. For this purpose, LES are carried out, and the wake flow is sampled and analysed at various fixed downstream positions.

Sect. 3.1 describes the general structure of the simulation, Sect. 3.2 describes the turbulent fluctuations and Sect. 3.3 explains the generation of the two different wake flows.

3.1 Numerical setup

The analysis in this work is carried out using LES simulations performed with OpenFOAM v2306 (OpenCFD, 2023). The domain has a size of 1890 m $\times$ 1024 m $\times$ 1024 m ($\approx$ 15 D $\times$ 8 D $\times$ 8 D). In the center, where the wake is present, the cells have a size of 1 m, which is fine enough to resolve intermittent turbulence (Bock et al., 2024b, a). Further out, the cells become larger, as the wake does not reach them and to reduce the computational cost. The mesh refinement follows a pattern similar to that used in Bock et al. (2026), resulting in a total of 263 million cells.

The numerical setup applies the Pimple algorithm (Greenshields and Weller, 2022) for pressure-velocity coupling, with two outer and two inner loops. A second-order backward scheme was used for the time and a second-order linear upwind scheme for the convective term. The standard Smagorinsky subgrid model (Smagorinsky, 1963) is used to represent unresolved subgrid-scale turbulence.

3.2 Turbulent field

For the turbulent inflow, a synthetic field from the Mann model (Mann, 1994, 1998; Liew et al., 2023; Liew, 2022) is used. As in Bock et al. (2026), the aim is to achieve a flow with homogeneous isotropic turbulence (HIT) and a realistic TI. The rotor diameter (126 m) is used as length scale. Instead of parameterising $\alpha\epsilon^{2/3}$ for the viscous dissipation, the field is scaled to a target TI, as suggested by Larsen and Hansen (2007). For the TI, a value of 5% is used, see Schubert et al. (2025). To obtain an isotropic flow, $\Gamma = 0$ is used. The field is as wide and high as the LES domain and has a length of 16,400 m, which corresponds to 1440 s. The resolution of the inflow field is 2 m, i.e. twice the LES resolution in the center of the domain, as suggested by Troldborg et al. (2014).

3.3 Turbine incorporation

When analysing a turbulent flow, the evaluation time must be long enough for the statistics to be converged (Oliver et al., 2014; Russo and Luchini, 2017). This is particularly important when analysing intermittency, as in this work, since this property is defined by rare extreme-events. The work of Lenschow et al. (1994) shows that the second to fourth moments of velocity

https://doi.org/10.5194/wes-2026-71
Preprint. Discussion started: 29 May 2026

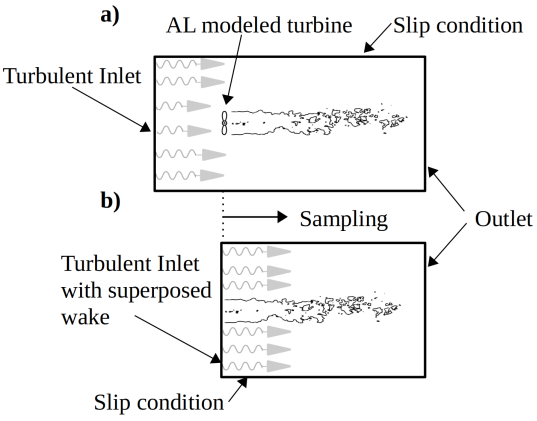

Figure 1. Schematic sketch of the LES for the AL case with turbulent inflow in a) and the superposed BR wake and synthetic turbulence in b).

converge from an evaluation length of 100 times the integral time ($\tau_{int} = L_{Int}/U_\infty$) in atmospheric turbulence. Consequently, based on the integral time of $\tau_{int} = 11.0$ s in the present case, this corresponds to a minimum simulation time of 1100 s. A total of 1200 s are analysed, which is twice the analysis period recommended in the IEC standard (IEC, 2019). A convergence study of the evaluation length is shown in Appendix A.

In general, a wind turbine can be modelled in a LES in various ways: by using an actuator disc (AD), an actuator line (AL) or fully blade-resolved (BR) model. Only AL and BR can reproduce a correct flow field in the near wake, see (Stoevesandt et al., 2022). This model enumeration corresponds to an increasing level of fidelity and calculation effort (BR is 33 times as costly as AL (Bock et al., 2026)). Due to the large computational effort required for BR, the common evaluation or averaging times of regular simulations are $< 150\ s$ (Dose et al., 2018; Guma et al., 2021; Grinderslev et al., 2021; Höning et al., 2024) and thus about one order of magnitude too short for the required convergence of the turbulence statistics.

This study utilises and compares two different methods (AL and BR) to evaluate the influence of the turbine modelling approach. The first is a classical AL method, with a turbulent inflow, as is commonly used (Figure 1 a). To achieve the required simulation length for the BR method, the following procedure is used (Figure 1 b). In a laminar BR precursor-simulation, the near wake flow field at 2 D downstream the turbine is sampled (Figure 2 a).This wake flow is sampled for six revolutions of the turbine ($\approx 30\ s$), so the blade positions are identical at the beginning and the end of the sampling period. This time series is repeated periodically to create a phase-connected wake field. The wake field is then superposed with the synthetic turbulent field (Figure 2 c), in an intermediate step. This approach is analogous to classical wake models, which superpose a velocity deficit onto the background flow field, cf. Göçmen et al. (2016). This field is then used as a time-varying inlet condition in the main simulation (Figure 1 b). The disadvantage of this method is that interaction between the wake and turbulence only occurs in the main simulation, starting 2 D downstream the turbine.

https://doi.org/10.5194/wes-2026-71
Preprint. Discussion started: 29 May 2026

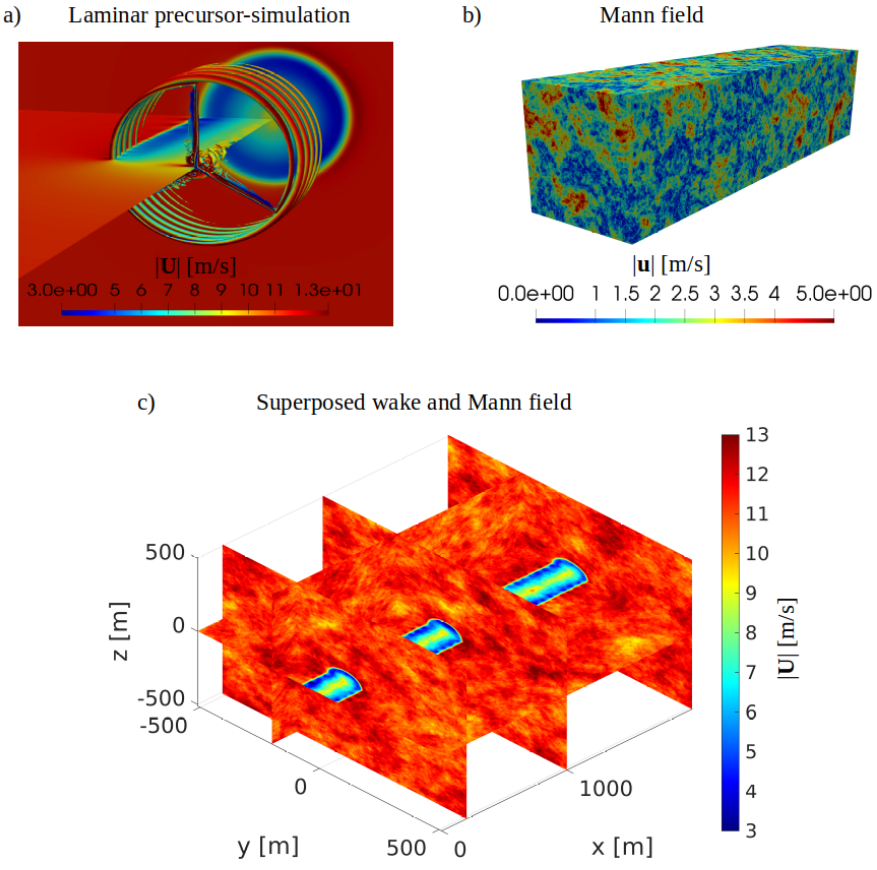

Figure 2. Schematic representation of the inflow condition for the BR case (Figure 1 b). Laminar precursor-simulation with visualised sampling plane and tip vortices through iso-surfaces of the Q criterion in a). Synthetic turbulence from the Mann model in b). Superposition of the sampled wake and synthetic turbulence in c).

4 Results and discussion

Next, we present the analysis of the AL and BR wake simulations. The results concerning turbulent features of the wakes are presented in accordance with the procedure described in Sect. 2.2, see also Morales et al. (2012). It starts with one-point statistics in Sect. 4.1 and self similar profiles of the one-point statistics in Sect. 4.2. It is followed by two-point statistics and
175 velocity increment analysis in Sect. 4.3. Finally, there is a comparison between the one- and two-point statistics in Sect. 4.4.

4.1 Wake characterisation from the velocities

To analyse the features of the wakes, we start with the statistics of the velocities themselves or, respectively, with the one-point analysis introduced above. The first four statistical moments of the velocities are analysed for different positions downstream the AL or BR modelled turbine. Figure 3 shows the results of the wake structures for the different moments, exemplary at 3 D.

https://doi.org/10.5194/wes-2026-71
Preprint. Discussion started: 29 May 2026

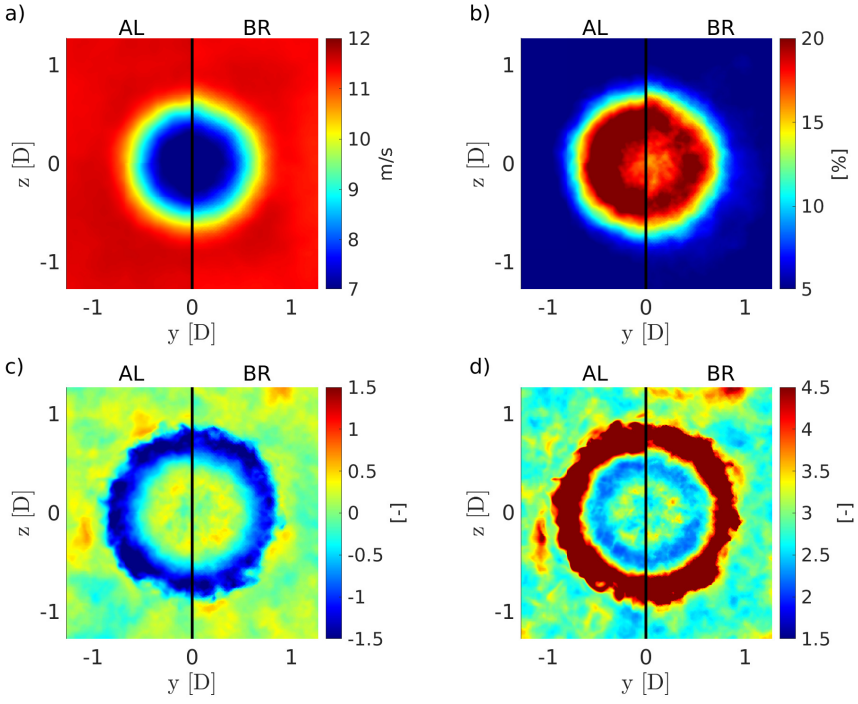

Figure 3. Comparison of the results of the simulations 3 D downstream the turbine for the AL (left) and BR (right) in each figure part. The sub-figures show the mean in a), the TI in b), the skewness in c), and the kurtosis in d).

The results from the AL case and the BR case are presented as opposing half wakes on the left and right sides, respectively (the corresponding figures for 6 D and 8 D are presented in Appendix B).

The mean velocity shows the typical behaviour of a wind turbine wake, with a round velocity deficit in the center. For the second moment, a TI of 5% is observed in the free stream region. In the wake itself, the TI is almost four times greater due to the turbulent mixing processes. These results are consistent with previous studies, as shown in Chamorro and Porté-Agel (2009); Maeda et al. (2011); Neunaber et al. (2017).

With a skewness of around zero and a kurtosis of around three, the pure synthetic turbulence outside the wake is Gaussian distributed. A similar behaviour can also be observed in the center of the wake. Further outside, in the wake, significantly lower values for skewness and higher values for kurtosis can be observed, which will be explained later.

The two different wake-generation methods, consisting of AL and superposed BR, do not indicate any qualitative differences. This does not imply that further details of the turbulent wake structure must be similar, too. Thus, both methods will be evaluated and compared also in the subsequent analyses.

For a quantitative comparison, the variation of the statistical moments is analysed over the radial position in the next step. This is done first for the BR case in detail (see Figure 4), followed by a shorter presentation of the AL results.

https://doi.org/10.5194/wes-2026-71
Preprint. Discussion started: 29 May 2026

eawe european academy of wind energy
Open Access WIND ENERGY SCIENCE DISCUSSIONS

At 1 and 2 D, the velocity profile follows a typical double Gaussian wake (Schreiber et al., 2020). As described by the double Gaussian wake model, the velocity profile converges towards a single Gaussian wake from 3 D on. The TI follows a comparable pattern in all positions. Outside the wake, there is a TI of 5%, which corresponds to the synthetic turbulence, while the wake itself exhibits a higher standard deviation and a continuous transition region that widens further downstream.

The skewness and kurtosis show clearly recognisable minima and maxima from 2 D onwards, which decrease in magnitude and increase in radial position the further away they are from the inlet.

The apparent radial structures of Figure 3 support the idea to discuss the radial wake size, which is often evaluated in wake studies. We define the end of the wake in radial direction at 2.5 standard deviations of the Gaussian profile of the velocity deficit (marked by the horizontal black dotted lines in Figure 4). By this definition, the wake contains 99% of the momentum and corresponds to a velocity at the edge of $0.983\ U_\infty$. Given this wake size, there is a consistent scaling behaviour of the statistical moments of the velocity. This radial position lies slightly outward of the turning point of the TI curve (shown by the black dots). Furthermore, it coincides with the minimum skewness, and the maximum kurtosis is located slightly further outward. In principle, one could also use any of the other variables in the same way instead of the velocity. However, as will be shown later, this does not matter.

To better understand the maximum kurtosis and minimum skewness, the PDF of the velocity is determined for three radial positions (see Figure 5). The central position in black represents the radius of the wake edge as defined by us as 98.3% U_∞ (dashed line in Figure 4). The two other positions are 0.16 D further inwards (red) and 0.16 D further outwards (blue). As expected, based on the corresponding mean values, the velocities are higher the further out the PDF is determined.

The inner distributions explain the origin of the maximum kurtosis and minimum skewness observed at the wake edge. At the wake edge, the distribution is heavy-tailed (kurtosis > 3) and left-skewed (skewness < 0). This results from the wake meandering in a turbulent environment, as sketched in Figure 1, see Larsen et al. (2007). As a result, the instantaneous wake center can be located at the radial position of the wake edge. If this is the case, very low velocities of 60% U_∞ occur there, which leads to a non-Gaussian, left-skewed distribution.

Following the result of the BR case, the AL results are shown in the same manner, to show the consistency of the different simulation methods. Figure 6 shows the statistical moments for the AL simulation plotted over the radius. The same features are evident as in the BR simulation: Gaussian distribution of the velocity deficit, higher TI in the centre, minimal skewness and maximum kurtosis at the end of the wake. As in the BR case, a clear double Gaussian velocity profile can be seen in near wake. At 1 D, the velocity at the centre is substantially greater than in the BR case. This is due to the modelling of the nacelle and is a known characteristic of AL simulations, see Churchfield et al. (2017).

4.2 Self-similarity in the velocity statistics

Self-similarity is a very important concept for the description of wake flows (Hinze, 1959) and has also been used for the velocity deficit and TI profile of wind turbine wakes (Johansson et al., 2003; Dufresne and Wosnik, 2013; Bastankhah and Porté-Agel, 2014; Ishihara and Qian, 2018). The results from Figure 4 and Figure 6 pose the question if this can also be used for skewness and kurtosis. To investigate this, these profiles are now presented in a normalised form. For this purpose, the

https://doi.org/10.5194/wes-2026-71
Preprint. Discussion started: 29 May 2026

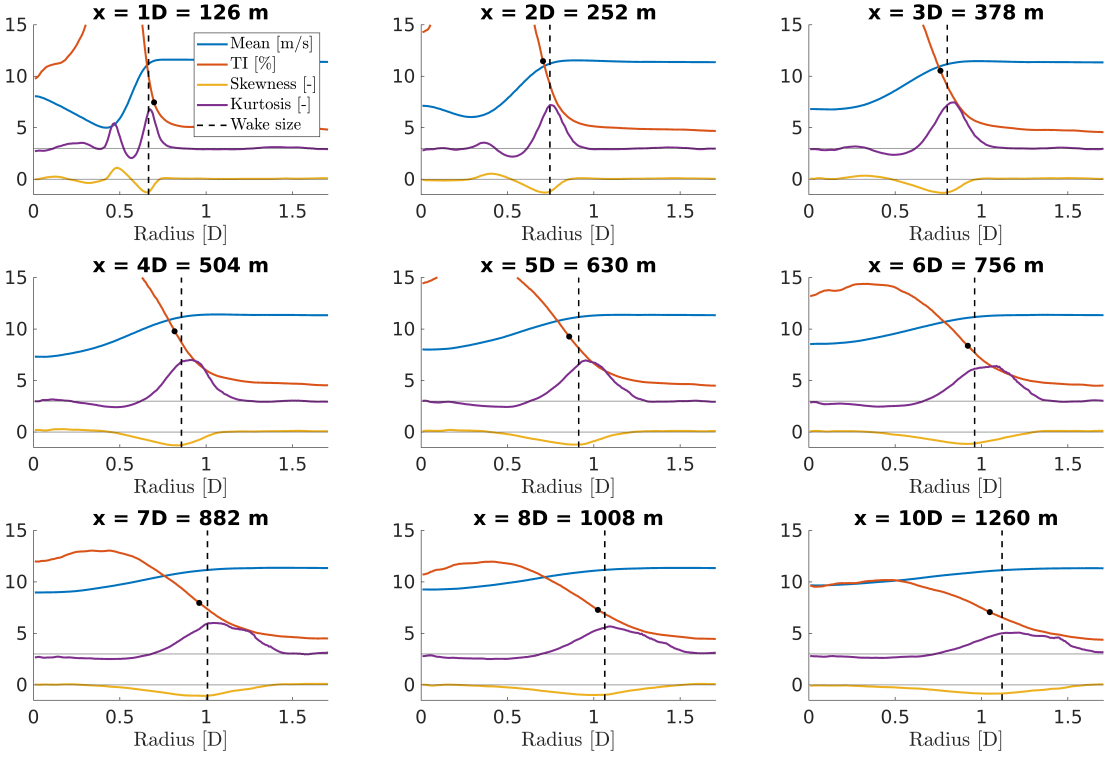

Figure 4. Statistical moments of the velocity at different downstream positions for the BR case. The black dotted line indicates the radial position at which 98.3% of the free stream velocity is reached. The black dot marks the numerical estimated turning point of the standard deviation.

absolute radii [m] are normalised to the wake size, r_{wake} (defined as 98.3% U_∞). As in Bastankhah and Porté-Agel (2014), the local velocity deficit is referenced to the maximum velocity deficit of the respective downstream position (Figure 7 a). The same procedure is also applied to the minimum skewness (Figure 7 c). By definition, the velocity deficit and skewness are 0 for the free stream, which is why this simple normalisation is possible. This is not the case for TI and kurtosis. Therefore, the difference to the free stream field value is first subtracted and then normalised to the maximum of the respective downstream position in Figure 7 b) and d). With this normalisation of amplitude and radius, the profiles for both cases AL and BR and all downstream positions from 4 D onwards show a tendency towards universal profiles.

The universal profiles can be regarded as first-order approximations. Deviations are seen in the normalized TI around the center for the AL case. Additionally, there is some variability in the center for the skewness and kurtosis. This is expected and results from the nacelle modelling and the root vortices, see Churchfield et al. (2017).

https://doi.org/10.5194/wes-2026-71
Preprint. Discussion started: 29 May 2026

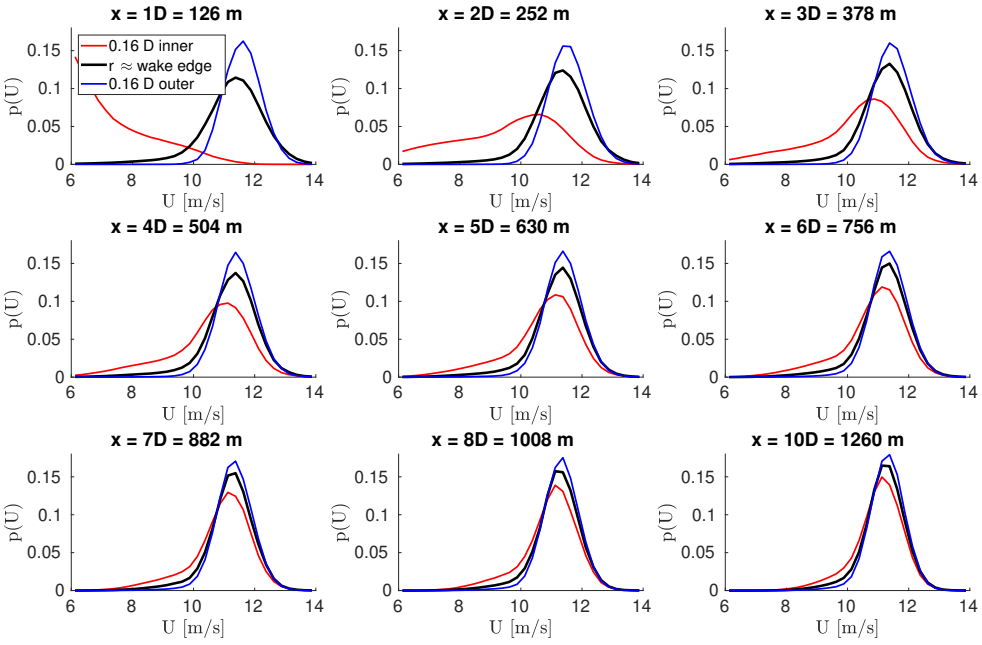

Figure 5. PDF of the velocity at three radial positions for different downstream positions for the BR case. Wake edge, defined as 98.3% of the free stream velocity (Figure 4) in black. 0.16 D inward in red and 0.16 D outward in blue.

4.3 Localised higher-order increment characterisation

The next step is to move from one-point to increment or two-point statistics. The increments can also be seen as a measure of the wind speed changes over the given time step, τ which may cause load variations or require actions of the control system of the wind turbine. As shown for example in Walgern et al. (2023) they are the disturbance that are compensated for by the critical pitch system of a wind turbine. Like in Sect. 4.1, the detailed description and evaluation of the results is first presented for the BR case. We focus on determining the local intermittency parameter, known from Sect. 2.2 as a key value.

Following the scheme of the two point characterisation from Sect. 2.2 the power spectra of the velocity signals are presented first in Figure 8 at three locations in the wake, namely the wake edge and 0.16 D inside and outside of it. These locations correspond to the locations of the velocity PDF in Figure 5. The spectra show, besides some differences in amplitude and shifts in the vertical direction, quite similar wavenumber and frequency dependencies. From this, we conclude that the variances of the increment PDF, $p(v(\tau))$ follow quite similar schemes.

Next we focus on the form of the increment PDF, $p(v(\tau))$, with the aim to investigate the intermittency of the flow. Therefore, a separate incremental analysis is carried out here for each of the 100,000 locations per evaluation plane. Figure 9 shows the increment PDF obtained for all locations in the plane (point-by-point for four different τ-values) for different downstream

https://doi.org/10.5194/wes-2026-71
Preprint. Discussion started: 29 May 2026

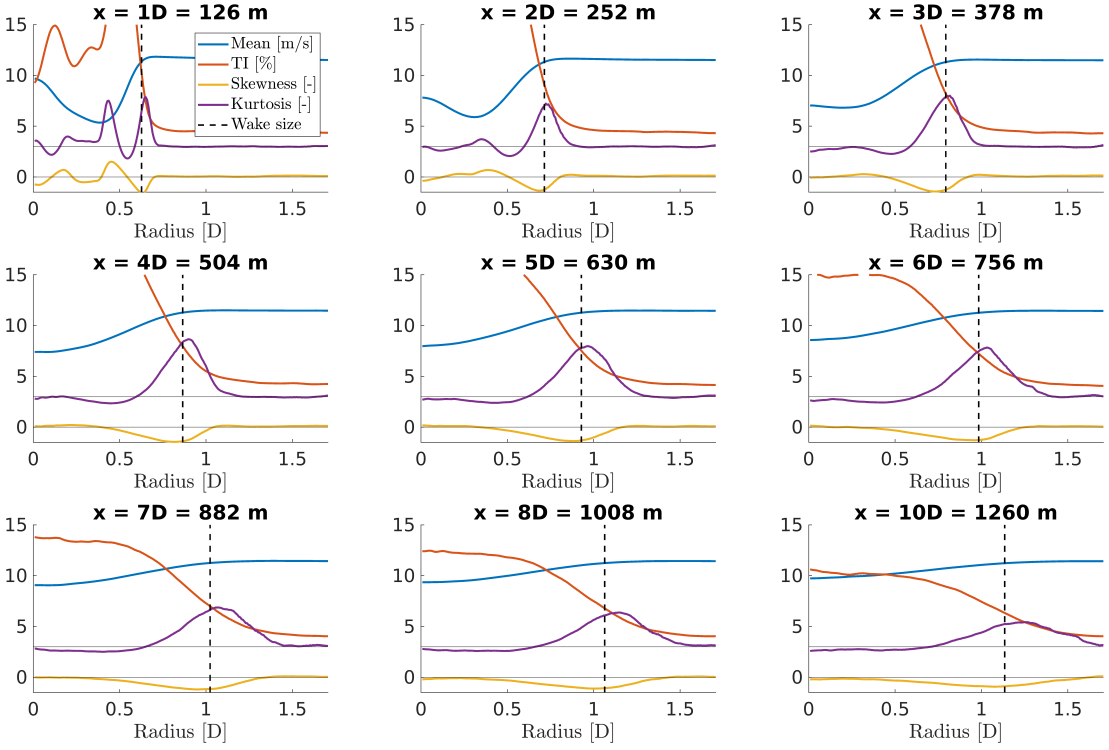

Figure 6. Statistical moments of the velocity at different downstream positions for the AL case. The black dotted line indicates the radial position at which 98.3% of the free stream velocity is reached. The black dot marks the numerical estimated turning point of the standard deviation.

positions. Due to the large number of PDFs, the lines are displayed with high transparency. In Appendix C there is the same analysis carried out for homogeneous isotropic turbulence as a reference.

The results for the different positions can be divided into two groups, starting with the positions between 2 D and 6 D. For the largest scale τ, (yellow), the data is noticeably scattered and almost Gaussian distributed. The scattering is stronger at the edges of the PDFs, which can be seen from the slight transparency. This scattering can have two reasons, on one hand for lower probabilities less events are used for their estimation and thus the probabilities become more noisy, on the other hand small deviations from Gaussianity becomes typically visible in these tails. The smaller the scale τ, the more the distributions deviate from a Gaussian distribution, with a higher probability of extreme events (so-called intermittency). Furthermore, the smaller the scale τ, the more clearly two distributions become apparent as darker curves in the PDFs, most noticeable at 3 D. The two distributions differ in their deviation from a normal distribution. This phenomenon of PDF clustering around two different distributions fades further downstream.

Concerning intermittency, a clear tendency is seen that beyond 4 D highly intermittent distribution dominates. This will be discussed later on in the context of an intermittency ring in the wake plane.

https://doi.org/10.5194/wes-2026-71
Preprint. Discussion started: 29 May 2026

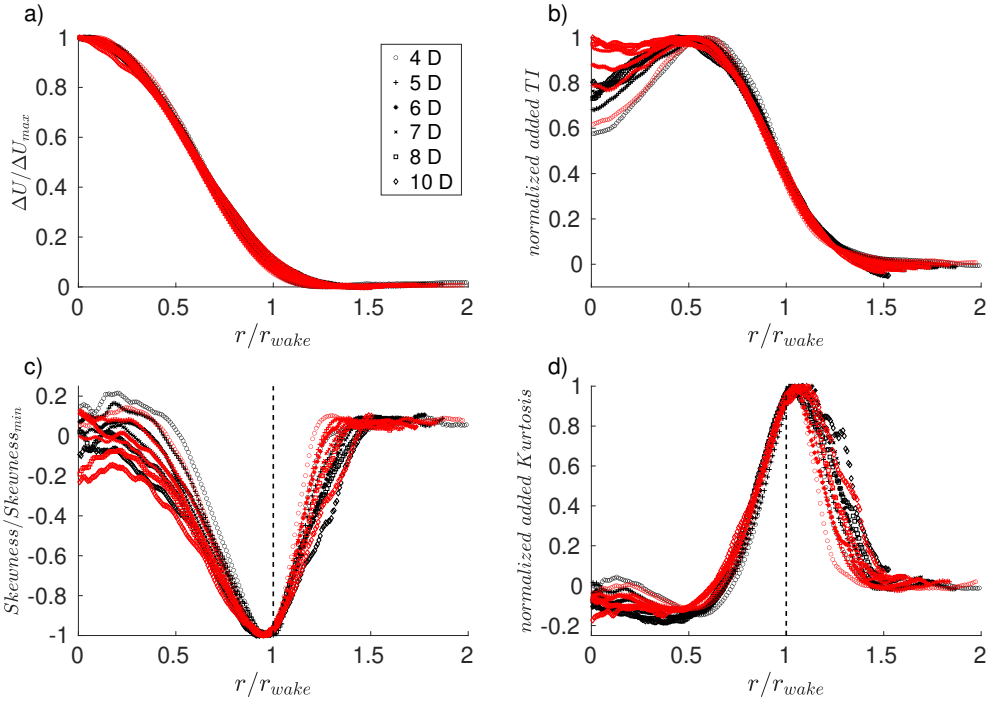

Figure 7. Normalised statistical moments of the velocity for the AL case (red) and the BR case (black) from 4 to 10 D. Different downstream positions represented by different markers for both cases.

In order to further confirm and better understand the findings described before regarding the mixed distributions, the shape parameter λ^2 is calculated according to the Castaing model Eq. (5) for each time series in the evaluation planes. Figure 10 shows the shape parameters over the scale τ, exemplary for 3 D. Thanks to the transparent representation of the lines ($\alpha_{plot} = 0.01$) the dominating portions can be identified, as those regions appear fully black or grey. There are two dominating portions present, as indicated by the red and blue lines.

According to the Castaing model, the intermittency parameter μ can be determined with a log-normal fit of the shape factor Eq. (6), as indicated in Figure 10. This approach has already been applied for both measurements (Boettcher et al., 2003; Morales et al., 2012) and LES simulations (Bock et al., 2024b, a) of atmospheric turbulence. These studies show values in the range of ideal (homogeneous and isotropic) turbulence, as suggested by Arneodo et al. (1996) of 0.26 ± 0.04. This method is now used for each time series.

Figure 11 shows the spatial distribution of the intermittency parameter at different downstream positions for the AL case on the left and the BR case on the right. From 2 D onwards, there is a clear ring-shaped structure with μ-values greater than 0.8. Such high values for the intermittency parameter have recently been reported and discussed in the context of non-ideal turbulence (Schmitt et al., 2024). Inside this ring, there is a homogenous field with values of $0.4 < \mu < 0.6$. Outside, there are lower values

https://doi.org/10.5194/wes-2026-71
Preprint. Discussion started: 29 May 2026

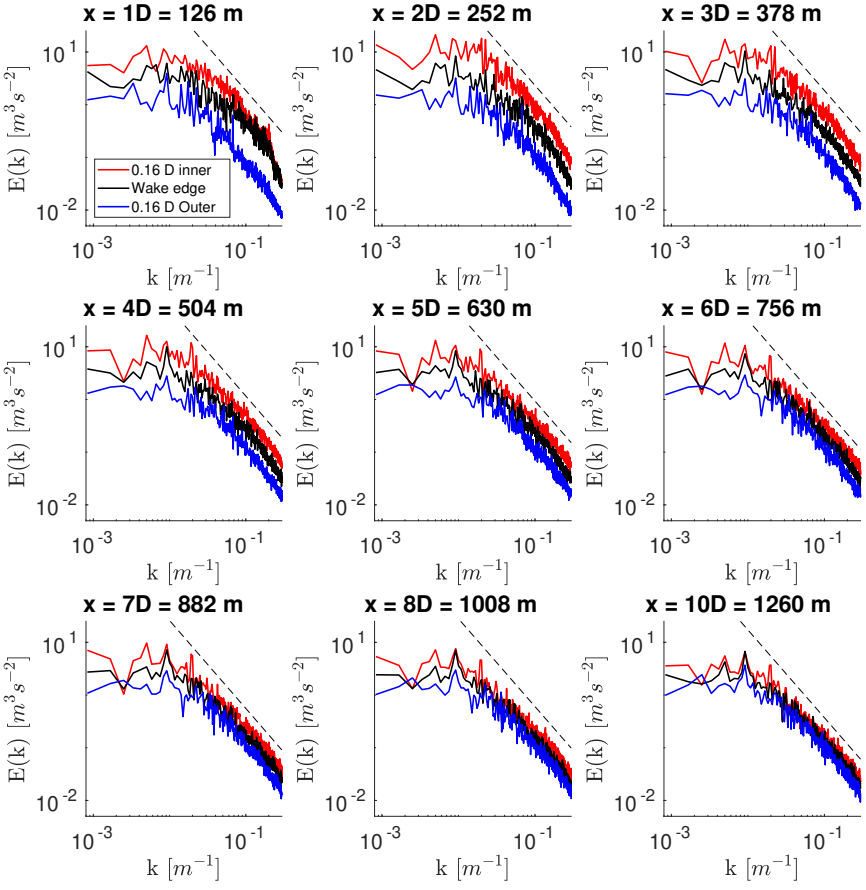

Figure 8. Power spectra of the velocities at the wake edge and 0.16 D inwards and outwards for different downstream locations. Data from the BR simulation.

https://doi.org/10.5194/wes-2026-71
Preprint. Discussion started: 29 May 2026

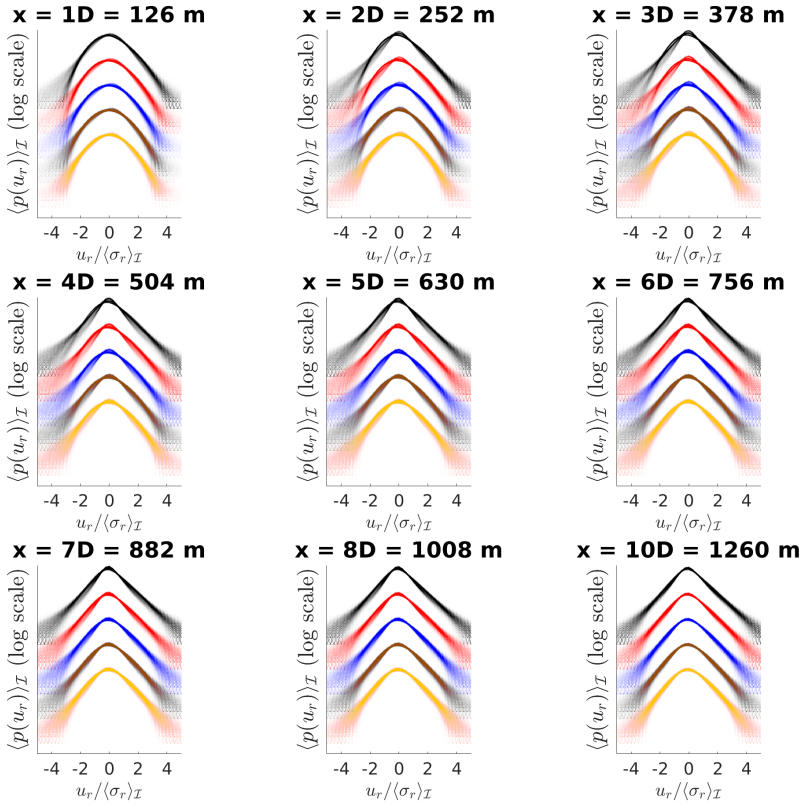

Figure 9. Velocity increment PDF for different scales τ and different downstream positions for the BR case. The PDFs are obtained from the individual time series of each point of the wake separately. PDF of the same scales τ are superimposed with the use of high transparency (α_{plot} = 0.005). According to τ values, the distributions are shifted horizontally for better visibility, with the smallest increment displayed as highest. The scales τ are 0.495 s, 1.16 s, 1.82 s, 2.48 s, and 3.14 s.

https://doi.org/10.5194/wes-2026-71
Preprint. Discussion started: 29 May 2026

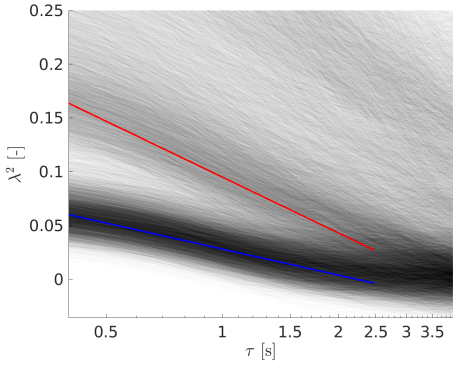

Figure 10. Point-by-point shape parameter λ^2 over the increment size τ, 3 D downstream the inlet (α_{plot} = 0.01). A log-normal relationship is indicated by the red and blue lines in the regions of dominant portions.

with $\mu < 0.3$. The radius of the ring grows continuously and from 5 D onwards and the μ-values within the ring decrease. This phenomenon of the so-called intermittency ring was already reported in the works of Neunaber (2019) and Vinnes et al. (2023). There, it was shown just by high values of λ^2 for one fixed scale τ corresponding via Taylor's frozen turbulence hypothesis to the diameter of the turbine.

In the near wake, at 1 D, clear differences in the ring structures and the free flow between AL and BR method is seen, obviously a consequence of our superposition ansatz for the BR model. The difference outside the wake region is a result of the different distance between the inlet and the sampling locations for the different inflow methods (see Figure 1). This distance for the inflow field is important as the Mann model is Gaussian and intermittency has to develop by transport and evolution through the LES, cf. Bock et al. (2024b). Thus, from 4 D onwards, the intermittency between AL and BR in the outside region become similar.

To confirm the validity of the intermittency parameter determination with Eq. (6), the increment PDF for the intermittency ring are determined for positions 2 D to 8 D of the BR case in Figure 12. In addition, fits to the PDFs using Castaing model (Eq. (4) are shown in blue. From the comparison of the empirical PDFs with the Castaing fits, it can be concluded that this approach provides a reasonably accurate characterization of the intermittency and is an essential improvement over a pure Gaussian approach often implicitly assumed. For example, if there is a threshold value for $v(\tau)$ that triggers a response from the control system, probability on such $v(\tau)$-events can be read off. In detail, the empirical PDFs are even more intermittent than the Castaing fits, particularly for 4 D, 6 D and 7 D. For 4 D we see the strongest deviation. Such a deviation is documented in an even more pronounced form in the experiments by Vinnes et al. (2023).

https://doi.org/10.5194/wes-2026-71
Preprint. Discussion started: 29 May 2026

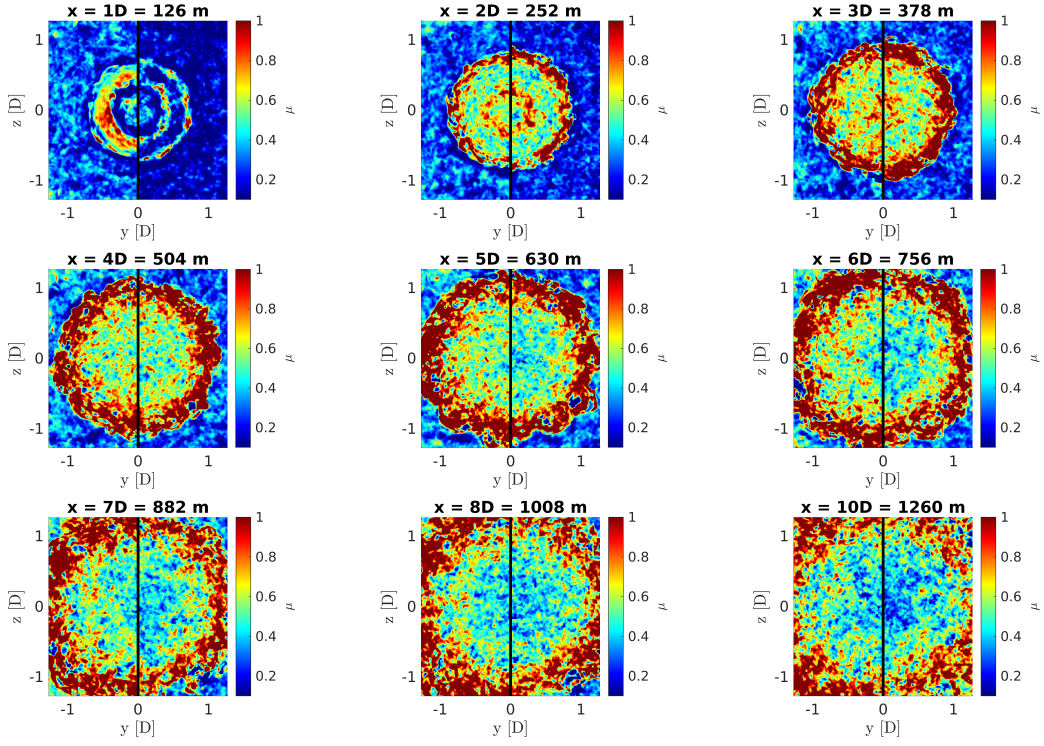

Figure 11. Spatial distribution of the intermittency parameter μ in wake for different downstream positions. The AL case is shown in the left and the BR case on the right.

4.4 Comparison of the wake characterisations

As a last point, the sizes of the different wake structures are compared with each other. In Sect. 4.1 and 4.2 it has been shown that the one-point statistics follow a common expansion governed by the radius of the mean velocity deficit. Figure 13 displays the downstream development of the wake size (mean velocity deficit) in full lines and of the intermittency ring in dashed lines, in black for the BR case and in red the AL case.

Due to the intermittent ring not yet being formed at 1 D and the intermittent ring partly protruding from the evaluation plane at 10 D, these two positions are omitted (see Figure 11).

As reference, a fit according to the linear propagation law of the Bastankhah wake model (Bastankhah and Porté-Agel, 2014) is added by the black dotted line. As predicted by the Bastankhah model, the wake expands linearly and matches the fit well ($R^2 = 0.982$). Here, a $k*$ parameter for the wake expansion rate is used with a value of 0.032, which is consistent with typical values (Zhan et al., 2020). Although the estimated radii of the intermittency rings are more noisy, it is clear that the intermittent ring expands faster than the wake radii of the one point velocity quantities. At 7 D the radius of the intermittency ring is approximately 350 m, about 1.5 times larger than the wake of the mean velocity. This is an important finding if one

https://doi.org/10.5194/wes-2026-71
Preprint. Discussion started: 29 May 2026

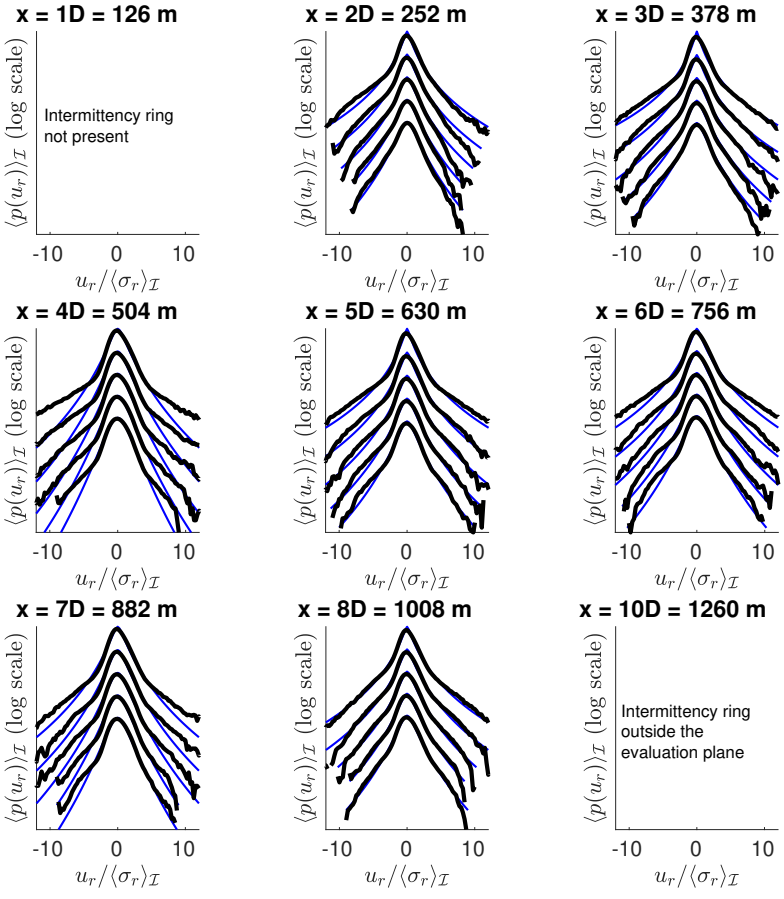

Figure 12. Velocity increment PDF for the intermittency ring for the BR case, shown for different downstream positions in black. Fits with the Castaing model in blue. The distributions are shifted horizontally for better visibility, with the smallest increment display as highest. The increment sizes are 0.495 s, 1.16 s, 1.82 s, 2.48 s, 3.14 s.

https://doi.org/10.5194/wes-2026-71
Preprint. Discussion started: 29 May 2026

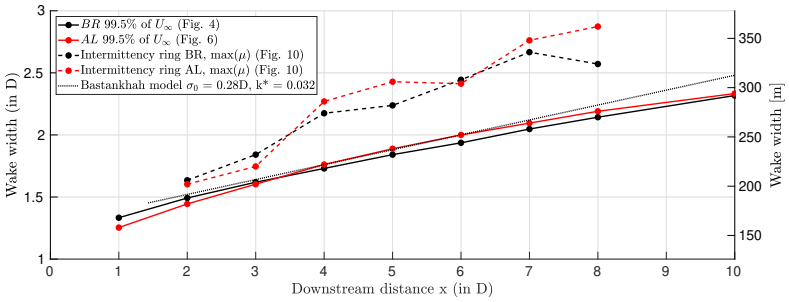

Figure 13. Wake width determined from the velocity (Figure 4 & Figure 6) shown by the full lines. Intermittency ring represented by the dashed lines (Figure 11). The BR case is shown in black and the AL case in red. Fit from the Bastankhah wake model for the wake size by the dotted line.

is interested in the impact of wakes on a downstream wind turbine. In this case, one has to pay attention that the real wake, including the intermittency ring, which is larger than commonly (without intermittency ring) expected.

5 Conclusions and Outlook

This paper investigates the development of wind turbine wakes in turbulent environments using LES by analysing the velocity and the velocity increment statistics.

Two different methods based on AL and BR were used for this purpose. Both methods have specific drawbacks but produce very similar results for the far wake (from 2 D onwards). Based on this cross-evaluation of the methods, it can be concluded that intrinsic flow characteristics of wind turbine wakes are described here.

A comparison of the computational effort for the two methods is not straightforward. The AL case is approximately 30% slower than the main simulation of the superposed BR case due to the calculation of the source terms and the resulting pressure coupling. However, in this cost comparison, the precursor simulation of a laminar turbine is not included. The flow field of the laminar wake is included in the supplementary material of this work. This means that the superposed inflow can easily be adopted for future work.

The first four statistical moments of the velocity (one-point statistics) follow universal profiles for multiple downstream positions for both methodologies. These profiles scale with the wake size, defined as 98.3% U_∞. The velocity deficit shows a transition downstream from a double-Gaussian profile (near wake) to a Gaussian profile (far wake) as introduced by Schreiber et al. (2020). Furthermore, at the radius of the mean velocity profiles coincide with the inflection point (second derivative zero) of the TI profiles, see also Ishihara and Qian (2018), with the minimum of the skewness (slightly shifted inward) and the maximum of the kurtosis (slightly outward).

Concerning the turbulent two-point characterisation of the wake, the intermittency ring described by Neunaber et al. (Neunaber, 2019; Vinnes et al., 2023) is confirmed. As an extension to previous work, it is shown that the intermittency ring is defined

https://doi.org/10.5194/wes-2026-71
Preprint. Discussion started: 29 May 2026

eawe european academy of wind energy
Open Access WIND ENERGY SCIENCE DISCUSSIONS

more generally for all scales τ and it is shown that the log-normal scaling behaviour is present. Thus, non-Gaussian increment statistics for different scales τ can be grasped by the intermittency parameter μ, from which an intermittency ring within the wake can be defined.

A comparison of the two wake characterisations (98.3% U_∞ and maximal μ) shows that the intermittency ring is located further outward than the edge of the wake. Furthermore, it expands faster than the velocity deficit. This can have important consequences for wind farms and wind turbines located downstream. This larger radius of the intermittency ring may be the reason that interaction between wakes starts already, although two wakes seem to be well separated based on their mean velocity radii. Similarly, a downstream wind turbine may already be affected by the wake, although its rotor is not inside the wake defined by the mean velocity deficit and TI. Whether the interaction of the wake's intermittency ring has an impact on a wind turbine is a subtle point, which has to be investigated in details. As a higher order statistical feature, the enhanced intermittency concerns mainly the speed of wind changes and their extreme values. Therefore, it has to be investigated if this may harm a turbine as suggested by Schottler et al. (2018).

Most wind turbine control models are based on the averaged velocity deficit. So a wind park may control the global flow field via wake steering in a way, that the wakes will not affect other turbines. However, the intermittency ring, i.e. an area with higher intermittency than the free stream turbulence and, therefore, an even greater probability of extreme events could hit the following turbine and cause increased ware to the drivetrain. Given this potential, future studies should also examine the influence of the intermittency ring on loads within wind farm control systems.

Appendix A: Convergence study

A convergence study is performed here to validate the evaluation length used based on the estimate of Lenschow et al. (1994). For this purpose, the length of the data set is varied from 10% of the total length to 100% in 10% increments (from 120 s to 1200 s). The velocity profile over the radius and the local intermittency parameter are determined for these intervals of varying lengths. This convergence study is performed on 3 D.

Figure A1 a) shows the radial velocity profile. In principle, the velocity for all evaluation lengths follows a Gaussian profile. The deviation between the individual velocity profiles and the longest evaluation interval is presented in Figure A1 b) and the average difference in Figure A1 c). From an evaluation length of 720 s onwards, the mean difference to the complete dataset is less than $0.02\ \mathrm{ms}^{-1}$.

https://doi.org/10.5194/wes-2026-71
Preprint. Discussion started: 29 May 2026

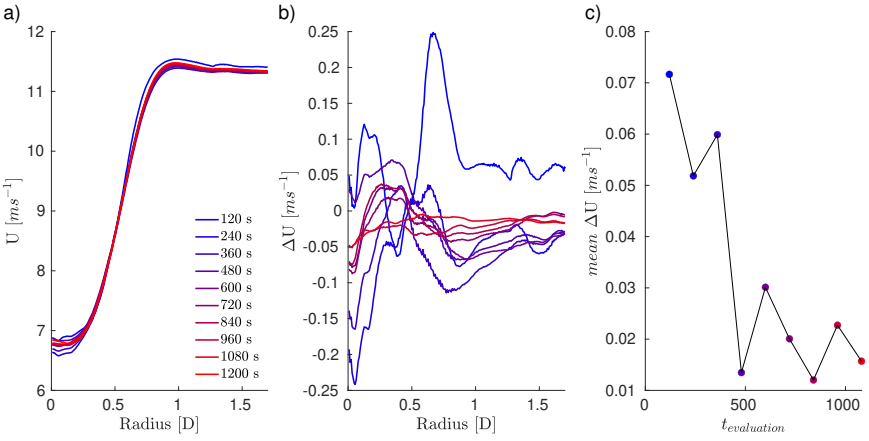

Figure A1. Convergence of the velocity profile at 3 D. Radial velocity profiles in a). Difference to the longest velocity profile over radius in b). Mean difference to the longest velocity profile in c).

Figure A2 shows the local intermittency parameter for the different evaluation lengths. Interestingly, an intermittency ring is already visible at an evaluation length of 120 s. Convergence is visible both for the area inside and outside the intermittency ring. For the shortest evaluation interval, the intermittency parameter is too low inside and too high outside.

In conclusion, the convergence study shows that the velocity exhibits the typical saturating behaviour. This characteristic is also present for local intermittency, but is not as easy to quantify.

https://doi.org/10.5194/wes-2026-71
Preprint. Discussion started: 29 May 2026

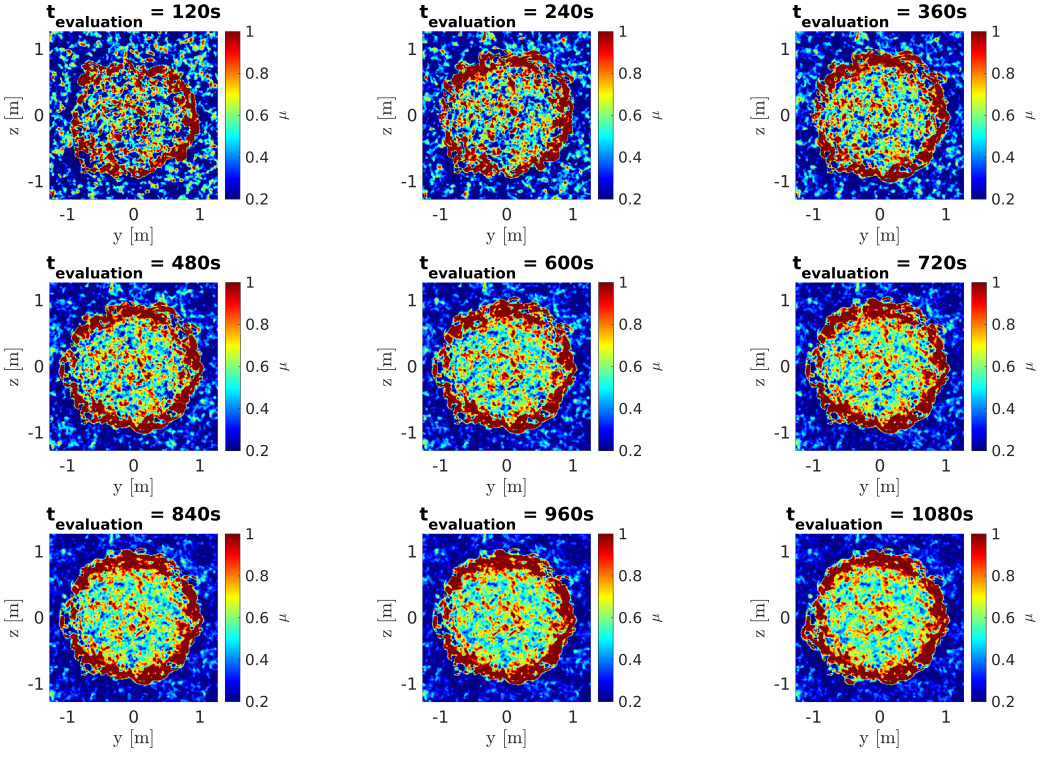

Figure A2. Local intermittency parameter at 3 D for different evaluation lengths.

Appendix B: Velocity statistics for additional downstream positions

This section shows the results from Sect. 4.1 Figure 3 for 6 D and 8 D.

https://doi.org/10.5194/wes-2026-71
Preprint. Discussion started: 29 May 2026

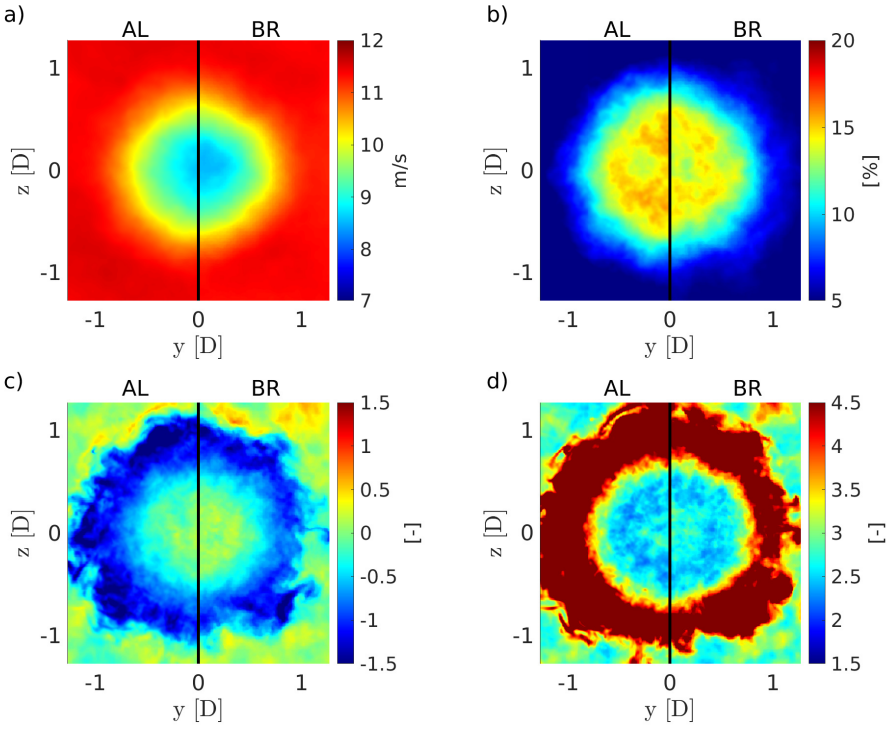

Figure B1. Comparison of the results of the simulations 6 D downstream the turbine for the AL (left) and BR (right) in each figure part. The sub-figures show the mean in a), the TI in b), the skewness in c), and the kurtosis in d).

https://doi.org/10.5194/wes-2026-71
Preprint. Discussion started: 29 May 2026

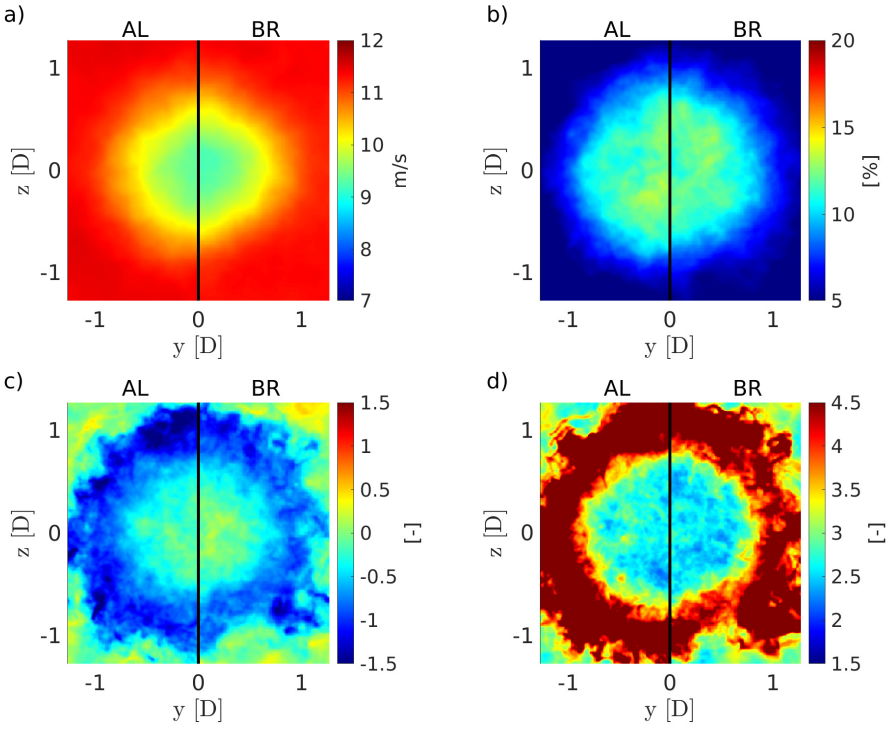

Figure B2. Comparison of the results of the simulations 8 D downstream the turbine for the AL (left) and BR (right) in each figure part. The sub-figures show the mean in a), the TI in b), the skewness in c), and the kurtosis in d).

Appendix C: Local intermittency in homogenous isotropic turbulence

This chapter analyses homogeneous isotropic turbulence without wake. First, a global analysis of all data is performed according to the methodology proposed by Fuchs et al. (2022). This is followed by a local analysis of the increments, as in the main part of this paper. This allows the methodology to be evaluated by comparing the local and global results.

370 At the same time, this analysis shows how intermittency develops locally in a homogeneous isotropic field from the Mann model in LES. Although these analyses are important and relevant, they would distract from the storyline on a wake flow in the main part of the paper, which is why they are presented in this detailed appendix.

Figure C1 shows the characterisation of global turbulence according to Fuchs et al. (2022), consisting of the single-point statistics (TI and energy spectrum in a) and b) and the higher order moments of the increments in c) and d), namely the shape

375 parameter λ^2 and the intermittency parameter μ.

https://doi.org/10.5194/wes-2026-71
Preprint. Discussion started: 29 May 2026

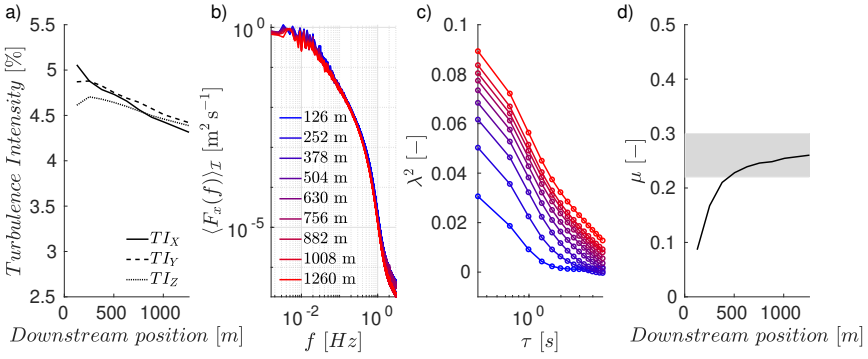

Figure C1. Basic characterisation of global turbulence. Turbulence intensity in a) Energy spectra in b) Shape parameter λ^2 of Increment size τ in c) and the intermittency parameter μ in d). The same colours were used in b) and c), and therefore the legend was described only once. The range of ideal turbulence according to Arneodo et al. (1996).

The typical behaviour of decaying (initially non-intermittent) turbulence in LES is evident. This means that the turbulence intensity decreases, the spectra remain relatively constant, and the flow becomes intermittent. The intermittency parameter converges towards a value of $\mu = 0.260$, which is exactly in the range of ideal turbulence as suggested by Arneodo et al. (1996) (marked by the grey box in d). Such behaviour has already been documented in (Bock et al., 2024a, b, 2026).

As in Figure 9 the increment PDFs for the individual sampling locations are determined. Figure C2 shows these PDFs for the different positions in LES downstream the inlet (also displayed with transparent lines; $\alpha_{plotting}$ = 0.005). In addition, dotted lines illustrate the global PDFs. For values around the center of the distribution ($\pm$ 2), the local distributions lay on top of each other and form solid full lines. Furthermore, these solid lines align with the global PDF.

At the edges, it can be seen that the lines scatter and a (visually) blurred area appears. This behaviour can be explained by the theory K62 turbulence model (Kolmogorov, 1962; Obukhov, 1962). This model states that energy dissipation fluctuates locally on small scales. As a result, when several areas of a turbulent domain are compared with each other, scatterings occur. In the work of Castaing et al. (1990), a connection between locally fluctuating energy dissipation and velocity increments was established, which is why the explanation of the K62 model can also be applied to the increments at this point. Due to the log-normal distribution of local dissipation, the scattering between the areas is most evident at the tails of the distribution.

https://doi.org/10.5194/wes-2026-71
Preprint. Discussion started: 29 May 2026

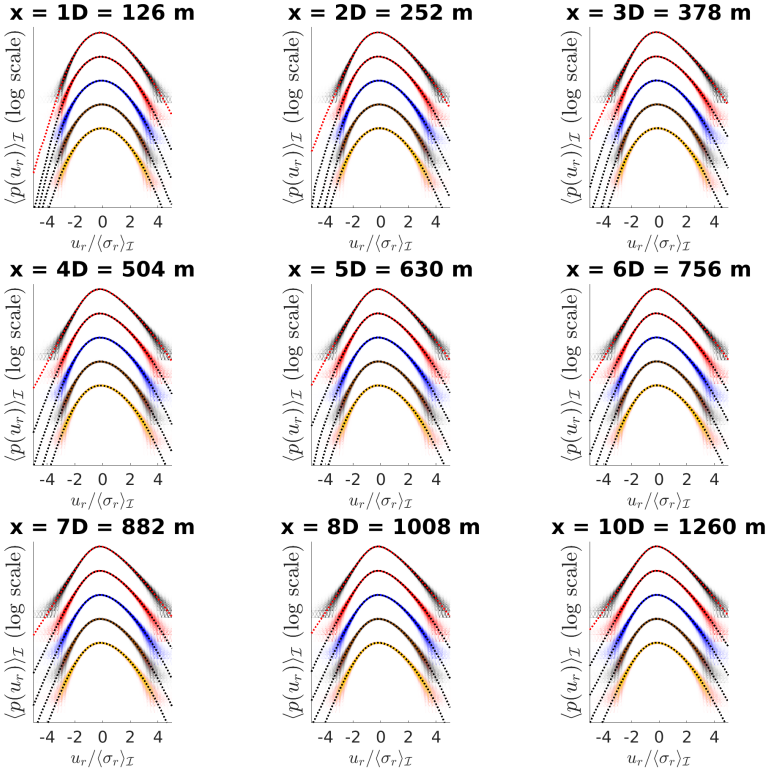

Figure C2. Local increment PDF for different downstream positions shown by the full transparent lines. Global PDF displayed by the dotted lines. The distributions are shifted horizontally for better visibility, with the smallest increment display as highest. The increment sizes are 0.495 s, 1.16 s, 1.82 s, 2.48 s, and 3.14 s.

As it can be seen from the Figure C1 in c) and d) the shape parameter follows a log-normal distribution as predicted by Kolmogorov (1962) and Castaing et al. (1990) and the intermittency parameter μ can be determined. Figure C3 shows the local shape parameters λ^2 in black (transparent) and the global ones in red. The majority of the local shape parameters are distributed around the global shape parameter curve, as can be seen in the dark areas. The local shape parameters vary, but it appears as they are parallel shifts around the global curve. There are also isolated outliers with values of $\lambda^2 > 0.1$ for the largest increment shown. All in all, the local shape parameter also follow a log-normal behaviour.

https://doi.org/10.5194/wes-2026-71
Preprint. Discussion started: 29 May 2026

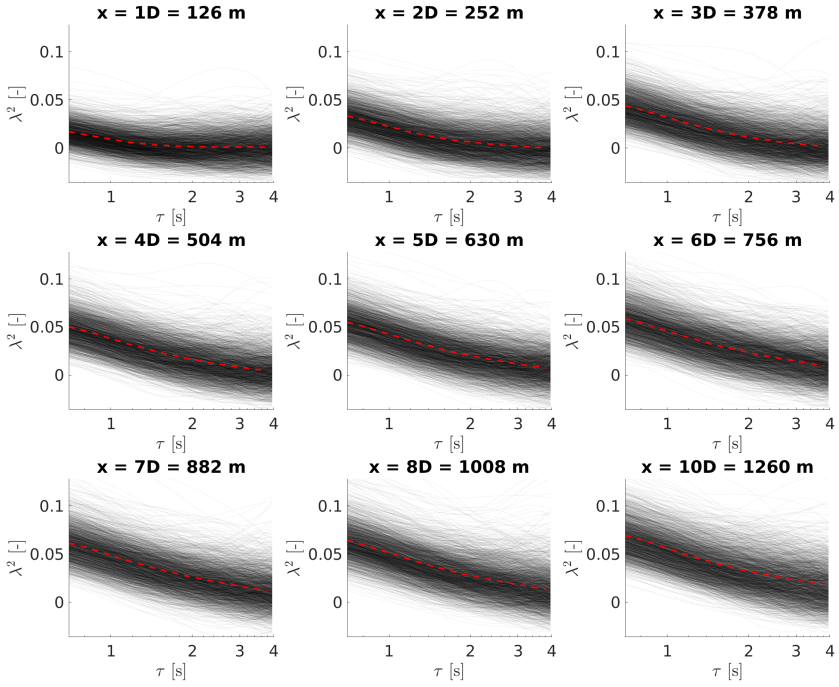

Figure C3. Shape parameter λ^2 for the increments for different downstream positions. The black and transplant lines represent the local values. The red dashed lines show the global values.

As a next step, the intermittency parameter is determined with the method of Chilla et al. (1996). Figure C4 shows the local intermittency parameter in the different evaluation planes. As with the increment PDF and the shape parameter, the values scatter due to the local fluctuation energy dissipation. Regardless of the scattering, the flow at 1 D is still largely Gaussian, with $\mu < 0.1$ and individual spots of higher values. At 2 D there is some sort of transition present, many spots of $\mu > 0.25$ but also many positions with $\mu < 0.15$. From 3 D onwards there is a clear intermittent state with most of the positions $0.2 < \mu < 0.4$.

https://doi.org/10.5194/wes-2026-71
Preprint. Discussion started: 29 May 2026

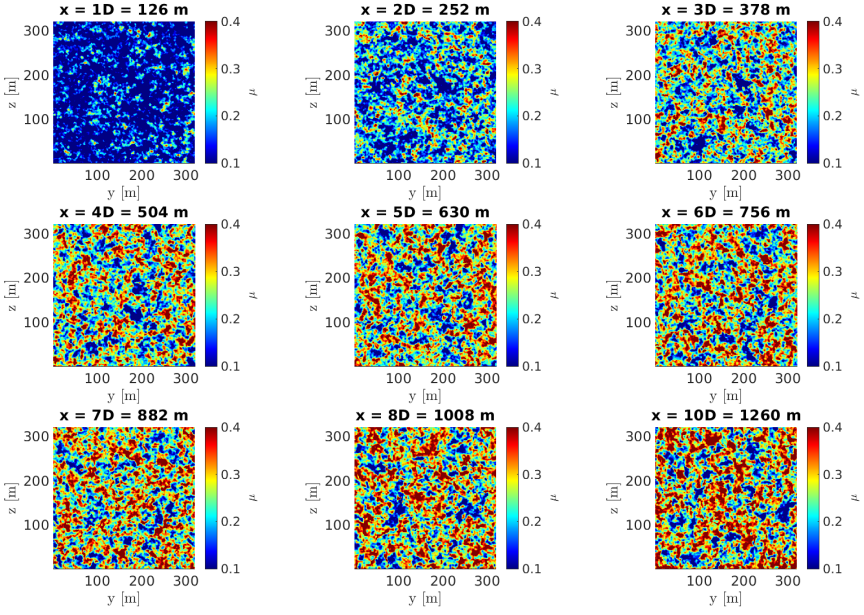

Figure C4. Local intermittency parameter for different downstream evaluation planes.

Since the local intermittency parameter only shows a homogeneous field, the statistics of the local intermittency are now analysed. In Figure C5 a) the PDFs of the local intermittency parameter from C4 for different downstream positions are shown. They all are fairly Gaussian, with increasing means and increasing standard deviations. As shown in Figure C3, there are a few areas in which no log-normal relationship between the shape parameter and the increment size is possible (or reasonable). These are areas in which the fits have very flat or even positive gradients. This circumstance results in negative intermittency parameters.

In Figure C5 b) the development of the mean of the local intermittency parameter over the downstream position is presented by the red line. Additionally, the global intermittency parameter is displayed in black. For reference, the range of ideal turbulence according to Arneodo et al. (1996) is shown by a grey box in both sub figures.

https://doi.org/10.5194/wes-2026-71
Preprint. Discussion started: 29 May 2026

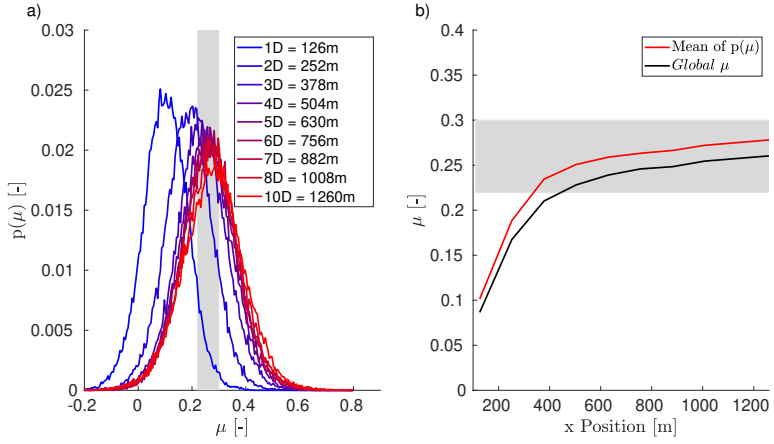

Figure C5. PDFs of the intermittency parameter in the evaluation planes (Figure C4) for different downstream positions in a). Development of the global intermittency parameter in black and the mean local intermittency parameter in red. Range of ideal turbulence according to Arneodo et al. (1996) shown by a grey box in both plots.

Code and data availability. All data created for this work was generated using open-source programmes. Nevertheless, a repository containing a test case of the simulation is available. This includes the sampled velocity field from the laminar BL simulation used in this work, a script for generating the inlet files, and a tailored OpenFOAM case. https://doi.org/10.57782/XOVL3Q (not yet the final link)

Author contributions. MB: conceptualisation, methodology, simulations, data analysis and calculations, writing – original draft. JP: supervision, writing – review and editing.

Competing interests. At least one of the (co-)authors is a member of the editorial board of Wind Energy Science.

Acknowledgements. This work was partially funded by the German Federal Ministry for Economic Affairs and Climate Action (BMWK) as part of the MOUSE project (FZK 03EE3067A). Computational resources of the University of Oldenburg were provided using the HPC cluster STORM, funded by the BMWK within the MOUSE project (FZK 03EE3067A). We acknowledge Neeraj Manelil for constructive discussions and feedback in the early stages of the writing process. The authors would like to acknowledge the assistance of large language models in refining the clarity and English-language style of a previous version of the paper. As non-native English speakers, this support helped improve the overall readability of the paper.

https://doi.org/10.5194/wes-2026-71
Preprint. Discussion started: 29 May 2026

eawe european academy of wind energy
Open Access WIND ENERGY SCIENCE DISCUSSIONS

References

Ali, N., Aseyev, A. S., Melius, M. S., Tutkun, M., and Cal, R. B.: Evaluation of higher order moments and isotropy in the wake of a wind turbine array, in: Whither turbulence and big data in the 21st century?, pp. 273–292, Springer, https://doi.org/10.1007/978-3-319-41217-7_15, 2016.

Arneodo, A., Baudet, C., Belin, F., Benzi, R., Castaing, B., Chabaud, B., Chavarria, R., Ciliberto, S., Camussi, R., Chillà, F., et al.: Structure functions in turbulence, in various flow configurations, atReynolds number between 30 and 5000, using extended self-similarity, Europhysics Letters, 34, 411, https://doi.org/10.1209/epl/i1996-00472-2, 1996.

Bartl, J., Pierella, F., and Sætrana, L.: Wake measurements behind an array of two model wind turbines, Energy Procedia, 24, 305–312, https://doi.org/10.1016/j.egypro.2012.06.113, 2012.

Bastankhah, M. and Porté-Agel, F.: A new analytical model for wind-turbine wakes, Renewable energy, 70, 116–123, https://doi.org/10.1016/j.renene.2014.01.002, 2014.

Beck, C.: Superstatistics: theory and applications, Continuum mechanics and thermodynamics, 16, 293–304, https://doi.org/10.1007/s00161-003-0145-1, 2004.

Bock, M., Fuchs, A., Friedrich, J., and Peinke, J.: The use of LES to analyse higher-order moments of two-point statistics, in: Journal of Physics: Conference Series, vol. 2767, p. 092080, IOP Publishing, https://doi.org/10.1088/1742-6596/2767/9/092080, 2024a.

Bock, M., Yassin, K., Kassem, H., Theron, J., Lukassen, L. J., and Peinke, J.: Intermittency, an inevitable feature for faster convergence of large eddy simulations, Physics of Fluids, 36, https://doi.org/10.1063/5.0202514, 2024b.

Bock, M., Moreno, D., and Peinke, J.: Comparison of different simulation methods regarding loads, considering the centre of wind pressure, Wind Energy Science, 11, 103–126, https://doi.org/10.5194/wes-11-103-2026, 2026.

Boettcher, F., Renner, C., Waldl, H.-P., and Peinke, J.: On the statistics of wind gusts, Boundary-Layer Meteorology, 108, 163–173, https://doi.org/10.1023/A:1023009722736, 2003.

Castaing, B., Gagne, Y., and Hopfinger, E.: Velocity probability density functions of high Reynolds number turbulence, Physica D: Nonlinear Phenomena, 46, 177–200, https://doi.org/10.1016/0167-2789(90)90035-N, 1990.

Chamorro, L. P. and Porté-Agel, F.: A wind-tunnel investigation of wind-turbine wakes: boundary-layer turbulence effects, Boundary-layer meteorology, 132, 129–149, https://doi.org/10.1007/s10546-009-9380-8, 2009.

Chilla, F., Peinke, J., and Castaing, B.: Multiplicative process in turbulent velocity statistics: A simplified analysis, Journal de Physique II, 6, 455–460, https://doi.org/10.1051/jp2:1996191, 1996.

Churchfield, M. J., Schreck, S. J., Martinez, L. A., Meneveau, C., and Spalart, P. R.: An advanced actuator line method for wind energy applications and beyond, in: 35th wind energy symposium, p. 1998, https://doi.org/10.2514/6.2017-1998, 2017.

Dose, B., Rahimi, H., Herráez, I., Stoevesandt, B., and Peinke, J.: Fluid-structure coupled computations of the NREL 5 MW wind turbine by means of CFD, Renewable energy, 129, 591–605, https://doi.org/10.1016/j.renene.2018.05.064, 2018.

Dufresne, N. P. and Wosnik, M.: Velocity deficit and swirl in the turbulent wake of a wind turbine, Marine Technology Society Journal, 47, 193–205, https://doi.org/10.4031/MTSJ.47.4.20, 2013.

Frisch, U.: Turbulence: the legacy of AN Kolmogorov, Cambridge university press, 1995.

Froude, W.: On the elementary relation between pitch, slip, and propulsive efficiency, Transactions of the Institution of Naval Architects, 19, 47–57, https://ntrs.nasa.gov/citations/19930080719, 1878.

https://doi.org/10.5194/wes-2026-71
Preprint. Discussion started: 29 May 2026

Fuchs, A., Kharche, S., Patil, A., Friedrich, J., Wächter, M., and Peinke, J.: An open source package to perform basic and advanced statistical analysis of turbulence data and other complex systems, Physics of Fluids, 34, https://doi.org/10.1063/5.0107974, 2022.

Göçmen, T., Van der Laan, P., Réthoré, P.-E., Diaz, A. P., Larsen, G. C., and Ott, S.: Wind turbine wake models developed at the technical university of Denmark: A review, Renewable and Sustainable Energy Reviews, 60, 752–769, https://doi.org/10.1016/j.rser.2016.01.113, 2016.

Greenshields, C. J. and Weller, H. G.: Notes on computational fluid dynamics: General principles, London, 2022.

Grinderslev, C., González Horcas, S., and Sørensen, N. N.: Fluid–structure interaction simulations of a wind turbine rotor in complex flows, validated through field experiments, Wind Energy, 24, 1426–1442, https://doi.org/10.1002/we.2639, 2021.

Guma, G., Bangga, G., Lutz, T., and Krämer, E.: Aeroelastic analysis of wind turbines under turbulent inflow conditions, Wind Energy Science, 6, 93–110, https://doi.org/10.5194/wes-6-93-2021, 2021.

Hinze, J. O.: Turbulence: An Introduction to Its Mechanism and Theory, Mcgraw-Hill, New York, ISBN 9780070290389, 1959.

Höning, L., Lukassen, L. J., Stoevesandt, B., and Herráez, I.: Influence of rotor blade flexibility on the near-wake behavior of the NREL 5 MW wind turbine, Wind Energy Science, 9, 203–218, https://doi.org/10.5194/wes-9-203-2024, 2024.

IEC: Wind energy generation systems –Part 1: Design requirements, IEC, Geneva, Switzerland, IEC 61400-1:2019-02 edn., 2019.

Ishihara, T. and Qian, G.-W.: A new Gaussian-based analytical wake model for wind turbines considering ambient turbulence intensities and thrust coefficient effects, Journal of Wind Engineering and Industrial Aerodynamics, 177, 275–292, https://doi.org/10.1016/j.jweia.2018.04.010, 2018.

Johansson, P. B., George, W. K., and Gourlay, M. J.: Equilibrium similarity, effects of initial conditions and local Reynolds number on the axisymmetric wake, Physics of Fluids, 15, 603–617, https://doi.org/10.1063/1.1536976, 2003.

Jonkman, J.: Definition of a 5-MW Reference Wind Turbine for Offshore System Development, National Renewable Energy Laboratory, https://doi.org/10.2172/947422, 2009.

Kolmogorov, A. N.: The local structure of turbulence in incompressible viscous fluid for very large Reynolds' numbers, Doklady Akademii Nauk SSSR, 30, 299–303, https://doi.org/10.1098/rspa.1991.0075, in Russian; English translation in Proc. R. Soc. Lond. A 434, 9–13 (1991), 1941.

Kolmogorov, A. N.: A refinement of previous hypotheses concerning the local structure of turbulence in a viscous incompressible fluid at high Reynolds number, Journal of Fluid Mechanics, 13, 82–85, https://doi.org/10.1017/S0022112062000518, 1962.

Larsen, G. C., Aagaard Madsen, H., and Bingöl, F.: Dynamic wake meandering modeling, Tech. Rep. Risoe-R-1607, Forskningscenter Risoe Denmark, https://backend.orbit.dtu.dk/ws/portalfiles/portal/7703042/ris_r_1607.pdf, 2007.

Larsen, T. J. and Hansen, A. M.: How 2 HAWC2, the user's manual, Risø National Laboratory, 2007.

Lee, S., Churchfield, M., Moriarty, P., Jonkman, J., and Michalakes, J.: Atmospheric and wake turbulence impacts on wind turbine fatigue loadings, in: 50th AIAA Aerospace Sciences Meeting including the New Horizons Forum and Aerospace Exposition, p. 540, https://doi.org/10.2514/6.2012-540, 2012.

Lenschow, D., Mann, J., and Kristensen, L.: How long is long enough when measuring fluxes and other turbulence statistics?, Journal of Atmospheric and Oceanic Technology, 11, 661–673, https://doi.org/10.1175/1520-0426(1994)011<0661:HLILEW>2.0.CO;2, 1994.

Liew, J.: jaimeliew1/Mann.rs: Publish Mann.rs v1.0.0, https://doi.org/10.5281/zenodo.7254149, 2022.

Liew, J., Riva, R., and Göçmen, T.: Efficient Mann turbulence generation for offshore wind farms with applications in fatigue load surrogate modelling, in: Journal of Physics: Conference Series, vol. 2626, p. 012050, IOP Publishing, https://doi.org/10.1088/1742-6596/2626/1/012050, 2023.

https://doi.org/10.5194/wes-2026-71
Preprint. Discussion started: 29 May 2026

Lledó, L., Torralba, V., Soret, A., Ramon, J., and Doblas-Reyes, F. J.: Seasonal forecasts of wind power generation, Renewable Energy, 143, 91–100, https://doi.org/10.1016/j.renene.2019.04.135, 2019.

Maeda, T., Kamada, Y., Murata, J., Yonekura, S., Ito, T., Okawa, A., and Kogaki, T.: Wind tunnel study on wind and turbulence intensity profiles in wind turbine wake, Journal of Thermal Science, 20, 127–132, https://doi.org/10.1007/s11630-011-0446-9, 2011.

Mann, J.: The spatial structure of neutral atmospheric surface-layer turbulence, Journal of fluid mechanics, 273, 141–168, https://doi.org/10.1017/S0022112094001886, 1994.

Mann, J.: Wind field simulation, Probabilistic engineering mechanics, 13, 269–282, https://doi.org/10.1016/S0266-8920(97)00036-2, 1998.

Morales, A., Wächter, M., and Peinke, J.: Characterization of wind turbulence by higher-order statistics, Wind Energy, 15, 391–406, https://doi.org/10.1002/we.478, 2012.

Mücke, T., Kleinhans, D., and Peinke, J.: Atmospheric turbulence and its influence on the alternating loads on wind turbines, Wind Energy, 14, 301–316, https://doi.org/10.1002/we.422, 2011.

Neunaber, I.: Stochastic investigation of the evolution of small-scale turbulence in the wake of a wind turbine exposed to different inflow conditions, Ph.D. thesis, Universität Oldenburg, 2019.

Neunaber, I., Schottler, J., Peinke, J., and Hölling, M.: Comparison of the development of a wind turbine wake under different inflow conditions, in: Progress in Turbulence VII: Proceedings of the iTi Conference in Turbulence 2016, pp. 177–182, Springer, https://doi.org/10.1007/978-3-319-57934-4_25, 2017.

Obukhov, A. M.: Some specific features of atmospheric tubulence, Journal of Fluid Mechanics, 13, 77–81, https://doi.org/10.1017/S0022112062000506, 1962.

Oliver, T. A., Malaya, N., Ulerich, R., and Moser, R. D.: Estimating uncertainties in statistics computed from direct numerical simulation, Physics of Fluids, 26, https://doi.org/10.1063/1.4866813, 2014.

OpenCFD: OpenFOAM: User Guide v2306, 2023.

Porté-Agel, F., Wu, Y.-T., Lu, H., and Conzemius, R. J.: Large-eddy simulation of atmospheric boundary layer flow through wind turbines and wind farms, Journal of Wind Engineering and Industrial Aerodynamics, 99, 154–168, https://doi.org/10.1016/j.jweia.2011.01.011, 2011.

Russo, S. and Luchini, P.: A fast algorithm for the estimation of statistical error in DNS (or experimental) time averages, Journal of Computational Physics, 347, 328–340, https://doi.org/10.1016/j.jcp.2017.07.005, 2017.

Sanchez Gomez, M. and Lundquist, J. K.: The effect of wind direction shear on turbine performance in a wind farm in central Iowa, Wind Energy Science, 5, 125–139, https://doi.org/10.5194/wes-5-125-2020, 2020.

Schmitt, F., Fuchs, A., Peinke, J., and Obligado, M.: A Universal Relation Between Intermittency and Dissipation in Turbulence, arXiv preprint, https://doi.org/10.48550/arXiv.2407.1595, 2024.

Schottler, J., Bartl, J., Mühle, F., Sætran, L., Peinke, J., and Hölling, M.: Wind tunnel experiments on wind turbine wakes in yaw: redefining the wake width, Wind energy science, 3, 257–273, https://doi.org/10.5194/wes-3-257-2018, 2018.

Schreiber, J., Balbaa, A., and Bottasso, C. L.: Brief communication: A double-Gaussian wake model, Wind Energy Science, 5, 237–244, https://doi.org/10.5194/wes-5-237-2020, 2020.

Schubert, C., Moreno, D., Schwarte, J., Friedrich, J., Wächter, M., Pokriefke, G., Radons, G., and Peinke, J.: Introduction of the Virtual Center of Wind Pressure for correlating large-scale turbulent structures and wind turbine loads, Wind Energy Science Discussions, 2025, 1–19, https://doi.org/10.5194/wes-2025-28, 2025.

https://doi.org/10.5194/wes-2026-71
Preprint. Discussion started: 29 May 2026

Schwarz, C. M., Ehrich, S., and Peinke, J.: Wind turbine load dynamics in the context of turbulence intermittency, Wind Energy Science, 4, 581–594, https://doi.org/10.5194/wes-4-581-2019, 2019.

Smagorinsky, J.: General circulation experiments with the primitive equations: I. The basic experiment, Monthly weather review, 91, 99–164, https://doi.org/10.1175/1520-0493(1963)091<0099:GCEWTP>2.3.CO;2, 1963.

Sørensen, J. N. and Kock, C. W.: A model for unsteady rotor aerodynamics, Journal of wind engineering and industrial aerodynamics, 58, 259–275, https://doi.org/10.1016/0167-6105(95)00027-5, 1995.

Stoevesandt, B., Schepers, G., Fuglsang, P., and Sun, Y.: Handbook of wind energy aerodynamics, Springer Nature, 2022.

Taylor, G. I.: The spectrum of turbulence, Proceedings of the Royal Society of London. Series A-Mathematical and Physical Sciences, 164, 476–490, https://doi.org/10.1098/rspa.1938.0032, 1938.

Troldborg, N., Sørensen, J. N., Mikkelsen, R., and Sørensen, N. N.: A simple atmospheric boundary layer model applied to large eddy simulations of wind turbine wakes, Wind Energy, 17, 657–669, https://doi.org/10.1002/we.1608, 2014.

Veers, P.: Modeling stochastic wind loads on vertical axis wind turbines, in: 25th Structures, Structural Dynamics and Materials Conference, p. 910, https://doi.org/10.2514/6.1984-910, 1984.

Vinnes, M. K., Neunaber, I., Lykke, H.-M. H., and Hearst, R. J.: Characterizing porous disk wakes in different turbulent inflow conditions with higher-order statistics, Experiments in Fluids, 64, 25, https://doi.org/10.18710/U4JMIV, 2023.

Von Karman, T.: Progress in the statistical theory of turbulence, Proceedings of the National Academy of Sciences, 34, 530–539, https://doi.org/10.1073/pnas.34.11.530, 1948.

Walgern, J., Fischer, K., Hentschel, P., and Kolios, A.: Reliability of electrical and hydraulic pitch systems in wind turbines based on field-data analysis, Energy Reports, 9, 3273–3281, https://doi.org/10.1016/j.egyr.2023.02.007, 2023.

Zhan, L., Letizia, S., and Iungo, G. V.: Optimal tuning of engineering wake models through lidar measurements, Wind Energy Science, 5, 1601–1622, https://doi.org/10.5194/wes-5-1601-2020, 2020.

Zheng, Y., Liu, H., Chamorro, L. P., Zhao, Z., Li, Y., Zheng, Y., and Tang, K.: Impact of turbulence level on intermittent-like events in the wake of a model wind turbine, Renewable Energy, 203, 45–55, https://doi.org/10.1016/j.renene.2022.12.052, 2023.